Near- and far-field evolution of laser pulse filaments in Kerr media

D. Faccio,[1,*] A. Matijosius,[1] A. Dubietis,[2] R. Piskarskas,[2] A. Varanavičius,[2] E. Gaizauskas,[2] A. Piskarskas,[2] A. Couairon,[3] and P. Di Trapani[1]

[1]*INFM and Department of Physics & Mathematics, University of Insubria, Via Valleggio 11, I-22100 Como, Italy*

[2]*Department of Quantum Electronics, Vilnius University, Sauletekio Ave. 9, bldg. 3, LT-10222 Vilnius, Lithuania*

[3]*Centre de Physique Theorique, Ecole Polytechnique, CNRS UMR 7644, F-91128 Palaiseau, France*

(Received 3 February 2005; revised manuscript received 16 June 2005; published 8 September 2005)

Measurements of the spatio-temporal and far-field profiles of ultrashort laser pulses experiencing conical emission, continuum generation, and beam filamentation in a Kerr medium outline the spontaneous formation of wave packets with *X*-like features, thus supporting recent numerical results [M. Kołesik, E. Wright, and J. Moloney, Phys. Rev. Lett. **92**, 253901 (2004)]. Numerical simulations show good agreement with experimental data.

DOI: 10.1103/PhysRevE.72.037601 PACS number(s): 42.65.Tg, 05.45.Yv, 41.20.Jb, 42.65.Jx

The dynamics of intense optical wave packets and the formation of apparently localized states in transparent nonlinear media have attracted major attention since the earliest stages of nonlinear optics [2–4]. The topic is still hotly debated, especially in view of forseeable applications [5,6] related to long-range self-channeling of ultrashort laser pulses in air [7–9], as well as for the interest of the localization process in different physical systems (e.g., Bose-Einstein condensates) which exhibit similar wave dynamics [10,11]. Solitons have been considered as the favored candidates for long-range, localized propagation. However, several mechanisms occur which make multidimensional (e.g. 2D spatial or spatiotemporal) solitons virtually inaccessible in real settings. Among these we quote spectral broadening, leading to important dispersive effects in normal group-velocity dispersion (GVD) (e.g., pulse splitting, self-steepening, etc.), and nonlinear losses (NLL) [12,13], which dominate in the case of 3D localization (in the regime of anomalous GVD). Preliminary experiments on spontaneous spatio-temporal localization in normal-GVD $\chi^{(2)}$ media raised the hypothesis of the existence of a stationary and weakly localized state substantially different from the spatiotemporal soliton, called the nonlinear X (NLX) wave [14], which appears as the exact stationary solution of both the $\chi^{(2)}$ and the nonlinear-Schrodinger-equation (NLSE) models [15]. NLX waves extend to the nonlinear regime the concept of linear X-waves, which are stationary and weakly localized wave packets (WP) in dispersive media made by the *coherent* (i.e., phase-locked) superposition of monochromatic Bessel beams with different frequencies at different cone angles [16]. An important characteristic of X-waves for their observation is that both the near and the far field exhibit a biconical shape. NLX waves belong to the general family of NL conical waves; other examples are the unbalanced Bessel beams (UBB) [17], in the monochromatic regime, and the nonlinear O-waves (NLO) [18], in the case of 3D spatiotemporal localization in anomalous GVD. The inherent robustness against nonlinear losses [17], a key feature of the NL conical wave, is a straightforward consequence of the self-regenerating property of the Bessel beam and plays an essential role in supporting the above-mentioned long-range propagation of the light filaments [19,20]. All these features make NL conical waves a very promising concept, alternative to the soliton, for understanding spontaneous dynamics and localization processes in several physical systems, ranging from optics to acoustics, spin waves, etc.

In optics, centrosymmetric materials are expected to exhibit a much more complex pulse propagation scenario than $\chi^{(2)}$ media, due to the higher saturation threshold that leads to the presence of higher-order dispersive and NL responses. This makes the prediction based on the simplest form of the NLSE model [15,21] (i.e., accounting only for Kerr nonlinearity, diffraction, and GVD) not necessarily adequate for modeling real physical systems. By examining the angular spectrum (θ,λ) of the evolving pulse as calculated from numerical simulations accounting also for plasma and higher-order dispersion, Kolesik *et al.* [1] have recently predicted spontaneous formation of X-waves for ultrashort-pulse propagation in water and interpreted the observed long-distance filamentation [22] in terms of X-wave dynamics. These results provide a relevant indication of the robustness of X-waves with respect to the presence of higher-order effects. However X-type angular spectra could be obtained as a consequence of the spatiotemporal modulational instability even in the absence of any regular, coherent (i.e. phase-locked) structure in the near field, as recently shown for the $\chi^{(2)}$ instability of extended waves [23]. These considerations leave the question of the spontaneous evolution from a Gaussian to an X-type wave packet (WP) in Kerr media still open. In this Brief Report, by using a nonlinear 3D mapping technique [24] we measure the wave-packet profile in the space-time domain, thus outlining the complicated dynamics, initially dominated by NLL, then by self-focusing and pulse splitting, finally leading to the formation of an X-like profile superimposed on a background of radiation generated by the initial dynamics.

In our experiments, filamentation was induced in the water sample by launching 160 fs pulses with wavelength centered at 800 nm. Similar measurements have been carried out

*Electronic address: daniele.faccio@uninsubria.it

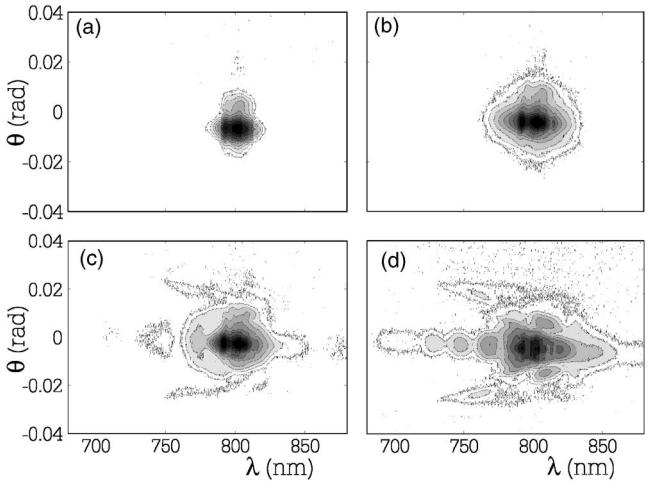

FIG. 1. Experimental (θ,λ) spectra for various water cell lengths (L). (a) Input pulse, (b) $L=1$ cm, (c) $L=2$ cm, (d) $L=3$ cm. The input energy is 3.3 μJ.

using a pump wavelength of 527 nm [25]. However, due to the nearer absorption band edge, NLL played an important role [26] and the GVD-dominated X-wave formation was difficult to highlight in the near-field, both experimentally and numerically, as also pointed out in [1]. The pulses were loosely focused onto the water-cell input facet with a 50 cm focal-length lens (the beam diameter at the cell input was 80 μm Full width at half-maximum) and an input energy of $E_{\text{in}}=3.3$ μJ. If we define the input critical power necessary to observe self-focusing as $P_{\text{crit}}=3.77\lambda^2/(8\pi n_0 n_2)$ $(\lambda, n_0, n_2 = 4.1\times10^{-16}$ cm^2/W are the vacuum wavelength, linear, and nonlinear material refractive indices, respectively) [27], then the input power is $P_{\text{in}}\sim 11P_{\text{crit}}$. An initial set of measurements was peformed in which we characterized the angular spectra (θ,λ) for various propagation lengths (L) by collecting the whole filament with a lens, placed so that the Fourier plane falls on the entrance slit of an imaging spectrometer (MS260i, Lot-Oriel). The output (θ,λ) spectrum is then recorded on a 16-bit CCD camera (DU420, Andor). Figure 1 shows the dynamics from the input pulse (a) to a generally widened spectrum at $L=1$ cm (b), followed by the appearance of colored conical emission, i.e., structures with a definite (θ,λ) dependence, at $L=2$ cm (c). Further propagation leads to an intense axial continuum generation at $L=3$ cm [Fig. 1(d)] along with the strengthening of the conical emission, with the appearance of X-like features, albeit with a marked asymmetry (the redshifted long X-tails seem to be missing). This angular dispersion results from the interplay between the Kerr nonlinearity, diffraction, and chromatic dispersion, or, analogously, from a strong space-time coupling. Therefore, a complete and correct characterization of the filamentation process, in the present regime, can only come from a full spatiotemporal mapping of the evolving WP profile. Note that this is a different regime with respect to previous experiments [17,20], which were dominated by purely spatial effects.

In order to perform such measurements, we resort to a new technique, called 3D mapping [24], that is based on a nonlinear optical gate and which has been used with success

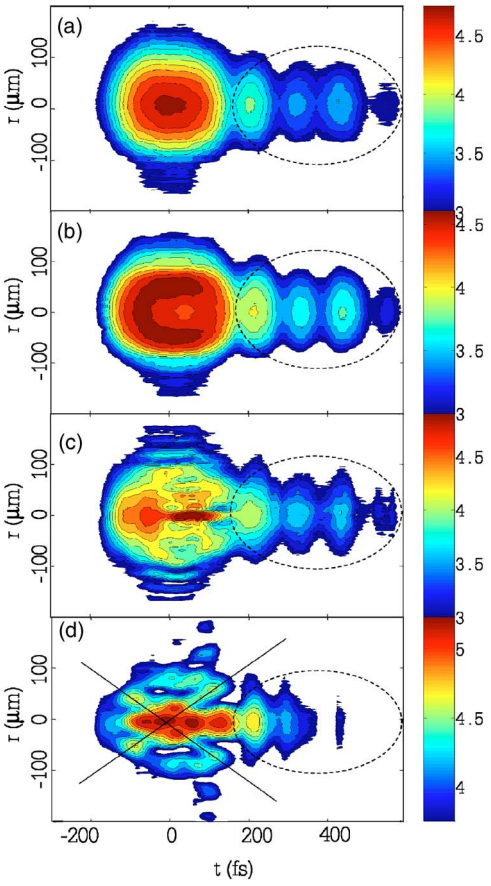

FIG. 2. (Color online) Experimentally measured space-time (r,t) profiles of a pulse in a Kerr medium (water) for different propagation distances in logarithmic scale (the shaded bar indicates the intensity-level decade): (a) input pulse ($\tau=160$ fs, diameter $=80$ μm), (b) $L=10$ mm, (c) $L=20$ mm, and (d) $L=30$ mm. Input energy is 3.3 μJ.

to characterize X-wave formation in $\chi^{(2)}$ materials [28]. Using this technique, we followed the pulse evolution by completing a measurement in the same input conditions of Fig. 1. Figures 2(a)–2(d) show the resulting space-time (r,t) intensity profiles for propagation distances of 0 cm (input beam), 1 cm, 2 cm, and 3 cm, respectively. The input pulse [Fig. 2(a)] is formed by a main peak, followed by a train of lower intensity satellite pulses, which appear due to the complex optical system specifically installed for locking the input laser-pulse energy at a fixed level, as mandatorily required for precise noise subtraction in the detection. These have been isolated by a dashed circle in all graphs as they do not participate in any of the nonlinear processes (note that they do not always seem to have the same intensity due to a residual fluctuating background noise related to unavoidable self-generated continuum emission). In the first cm of propagation [Fig. 2(b)], the pulse undergoes space-time reshaping featured by a notable depletion of the central peak, as expected from the effect of NLL and/or plasma defocusing. During the second cm [Fig. 2(c)], the pulse propagation is dominated by Kerr effects and a strong self-focusing is observed. Finally, at $L=3$ cm [Fig. 2(d)] we observe a trace of pulse splitting but also the formation of a symmetric

X-shaped structure (highlighted by solid lines) featured by a central peak and by characteristic bi-conical (clessidra-like) tails. We interpret the presence of a rather intense axial radiation at $t \neq 0$ as a residual effect of the pulse-splitting dynamics. Further measurements at greater propagation lengths were prevented by technical difficulties in subtracting white-light continuum from the SF signal.

In order to gain a deeper insight into the underlying dynamics, we have performed numerical simulations: here we briefly outline the model that is described in more detail elsewhere [29]. We model the linearly polarized beam with cylindrical symmetry around the propagation axis z by the envelope $\mathcal{E}$ of the electric field $\mathbf{E}$, written as $\mathbf{E} = \mathrm{Re}[\mathbf{i}\mathcal{E}\exp(ikz - i\omega_0 t)]$, where $\mathbf{i}$ is the unit polarization vector, and $k = n_0\omega_0/c$ and ω_0 are the wave number and frequency of the carrier wave. The input pulses are modeled by Gaussians with parameters taken so as to match the main near-field intensity peak, as measured experimentally [Fig. 2(a)]. The scalar envelope $\mathcal{E}(r,t,z)$ evolves along the propagation axis z according to the nonlinear envelope equation [30], expressed in the time domain as

$$\frac{\partial \mathcal{E}}{\partial z} = \frac{i}{2k} U^{-1} \nabla_\perp^2 \mathcal{E} - i\frac{k''}{2}\frac{\partial^2 \mathcal{E}}{\partial t^2} + \frac{k'''}{6}\frac{\partial^3 \mathcal{E}}{\partial t^3} + U^{-1} N(\mathcal{E}), \qquad (1)$$

where $U \equiv [1 + (i/kv_g)\partial/\partial t]$ and $v_g = \partial\omega/\partial k$. Equation (1) accounts for diffraction in the transverse plane, space-time focusing, second-, and third-order dispersion (with the relative coefficients taken from literature [31]). No redshift has been observed in the experiments and therefore no nonlocal term corresponding to delayed Raman-Kerr contribution is taken into account. Finally, the nonlinear term is

$$N(\mathcal{E}) = ik_0 n_2 T^2 |\mathcal{E}|^2 \mathcal{E} - \frac{\sigma}{2}(1 + i\omega_0\tau_c)\rho\mathcal{E} - T\frac{\beta_K}{2}\left(1 - \frac{\rho}{\rho_{\mathrm{at}}}\right) \times |\mathcal{E}|^{2K-2}\mathcal{E} \qquad (2)$$

and includes the optical Kerr effect with possible shock terms, plasma absorption, plasma defocusing, and multiphoton absorption. $\rho_{\mathrm{at}} = 6.7 \times 10^{22}$ cm^{-3} denotes the density of neutral molecules of water, $\rho = \rho(r,t,z)$ is the plasma electron density generated by multiphoton ionization according to $\partial\rho/\partial t = \sigma_K |\mathcal{E}|^{2K}(\rho_{\mathrm{at}} - \rho)$, with $\sigma_K = 1.2 \times 10^{-52}$ s^{-1}(cm^2/W)^5. $K = 5$ is the number of photons involved in the NL absorption process, $\beta_K = 10^{-47}$ cm^7/W^4 and $\sigma = 5.1 \times 10^{-17}$ cm^2 are the cross sections for multiphoton absorption and inverse brehmsstrahlung, respectively, $\tau_c = 3$ fs is the momentum transfer collision time, and the operator $T \equiv 1 + (i/\omega_0)\partial/\partial t$ is responsible for the self-steepening of the pulse.

Figure 3(a) shows the calculated (r,t) intensity profile after 3 cm of propagation. The scale has been chosen so as to match the experimental dynamic range, i.e., $\sim$2 decades. As can be seen, the numerically calculated profile matches the experimental one quite well, the main difference being that the central peak is not yet completely reformed. Figure 3(b) is a plot of the same graph but now over four decades in intensity, showing many low-intensity features that were not revealed experimentally. In particular, we note that the central X-like profile emerges as the peak of a vaster and weaker underlying structure. Indeed, Fig. 3(b) allows one to speculate that the conical features of Fig. 3(a) result from the interference and interaction of multiple, overlapping X-forms, born by multiple split-off pulses.

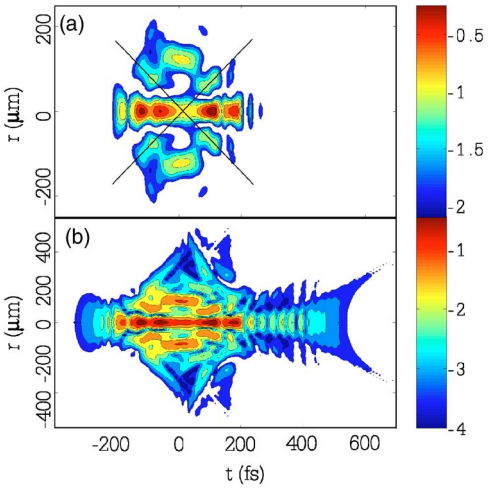

FIG. 3. (Color online) Numerical simulations in water at 800 nm. (a) Normalized space-time (r-t) intensity profile in logarithmic scale (two decades), in the same conditions as in Fig. 2(d) ($E_{\mathrm{in}} = 3.3$ μJ, $L = 3$ cm). (b) Same as in (a) but with intensity profile plotted over four decades showing much weaker X features.

These results suggest that the X-wave acts as an attractor in the dynamics of femtosecond pulse filamentation, while the pulse-splitting dynamics are a necessary step for permitting an initial bell-shaped intensity, flat-phase profile to evolve toward the X-type wave. We noticed that mutiple recycling takes place, in numerical experiments (see also [32]), when the wave packet still carries a strong memory of the initial input condition, with a phase profile differing substantially from that imposed by the conical geometry of the X wave. We finally note that a good qualitative agreement with the experiment was also obtained for the calculated spectra, with (θ,λ) intensity profiles similar to those shown elsewhere [1], referring to the 527 nm input-pulse case. An important difference is that here the pump wavelength is closer to the zero-dispersion point of water ($\sim$1000 nm) so that higher-order dispersive effects become important. Third-order dispersion is such that a marked asymmetry between the redshifted and blueshifted spectral X tails is observed, with the former being nearly absent, thus explaining the apparent anomaly (i.e., the missing redshifted CE) in the spectra in Figs. 1(c) and 1(d).

In summary, we have presented experimental measurements, supported by numerical simulations, that map the spontaneous transformation of a Gaussian laser pulse in a Kerr medium. Observing the near-field evolution, it is possible to highlight different dominating effects during the pulse propagation, leading, finally, to the formation of an X-shaped object surrounded by a complicated background. Indeed, our numerics indicate that the whole structure actually arises from a much broader underlying interaction between split-off daughter pulses. Each of these exhibit X-like

features, thus supporting the hypothesis [1] of spontaneous X-wave formation and interaction in Kerr media.

The authors gratefully acknowledge the support of F. Bragheri and Light Conversion Ltd. in measurements and financial support from FIRB01, COFIN04 projects from the Italian Ministry of University and Research (MIUR), and by the Access to Research Infrastructures activity in the Sixth Framework Programme of the EU (Contract No. RII3-CT-2003-506350, Laserlab Europe).

[1] M. Kolesik, E. M. Wright, and J. V. Moloney, Phys. Rev. Lett. **92**, 253901 (2004).
[2] G. Askarjan, Sov. Phys. JETP **42**, 1672 (1962).
[3] R. Y. Chiao, E. Garmire, and C. H. Townes, Phys. Rev. Lett. **13**, 479 (1964).
[4] M. Hercher, J. Opt. Soc. Am. **54**, 563 (1964).
[5] J. Kasparian *et al.*, Science **301**, 61 (2003).
[6] A. Gaeta, Science **301**, 54 (2003).
[7] A. Braun, G. Korn, X. Liu, D. Du, J. Squier, and G. Mourou, Opt. Lett. **20**, 73 (1995).
[8] G. Méhain, A. Couairon, Y. André, C. D'Amico, M. Franco, B. Prade, S. Tzortzakis, A. Mysyrowicz, and R. Sauerbrey, Appl. Phys. B: Lasers Opt. **79**, 379 (2004).
[9] T. Pitts, T. Luk, J. Gruetzner, T. Nelson, A. McPherson, and S. Cameron, J. Opt. Soc. Am. B **21**, 2008 (2004).
[10] K. Strecker, G. Partridge, A. Trscott, and R. Hulet, Nature (London) **417**, 150 (2002).
[11] L. Khaykovich, F. Schreck, G. Ferrari, T. Bourdel, J. Cubizolles, L. Carr, Y. Castin, and C. Salomon, Science **296**, 1290 (2002).
[12] H. S. Eisenberg, R. Morandotti, Y. Silberberg, S. Bar-Ad, D. Ross, and J. S. Aitchison, Phys. Rev. Lett. **87**, 043902 (2001).
[13] Y. F. Chen, K. Beckwitt, F. W. Wise, and B. A. Malomed, Phys. Rev. E **70**, 046610 (2004).
[14] G. Valiulis, J. Kilius, O. Jedrkiewicz, A. Bramati, S. Minardi, C. Conti, S. Trillo, A. Piskarskas, and P. Di Trapani, in *OSA Trends in Optics and Photonics (TOPS)*, Vol. 57, pp. QPD10 1-2 (2001).
[15] C. Conti, S. Trillo, P. Di Trapani, G. Valiulis, A. Piskarskas, O. Jedrkiewicz, and J. Trull, Phys. Rev. Lett. **90**, 170406 (2003).
[16] H. Sõnajalg, M. Rätsep, and P. Saari, Opt. Lett. **22**, 310 (1997).
[17] M. A. Porras, A. Parola, D. Faccio, A. Dubietis, and P. Di Trapani, Phys. Rev. Lett. **93**, 153902 (2004).
[18] M. Porras, A. Parola, and P. Di Trapani, J. Opt. Soc. Am. B **22**, 1406 (2005).
[19] A. Dubietis, E. Kucinskas, G. Tamosauskas, E. Gaizauskas, M. A. Porras, and P. D. Trapani, Opt. Lett. **29**, 2893 (2004).
[20] A. Dubietis, E. Gaižauskas, G. Tamošauskas, and P. Di Trapani, Phys. Rev. Lett. **92**, 253903 (2004).
[21] C. Conti, Phys. Rev. E **68**, 016606 (2003).
[22] A. Dubietis, G. Tamošauskas, I. Diomin, and A. Varanavičius, Opt. Lett. **28**, 1269 (2003).
[23] D. Salerno, O. Jedrkiewicz, J. Trull, G. Valiulis, A. Picozzi, and P. Di Trapani, Phys. Rev. E **70**, 065603(R) (2004).
[24] J. Trull, O. Jedrkiewicz, P. Di Trapani, A. Matijosius, A. Varanavičius, G. Valiulis, R. Danielius, E. Kucinskas, A. Piskarskas, and S. Trillo, Phys. Rev. E **69**, 026607 (2004).
[25] A. Matijosius, J. Trull, P. Di Trapani, A. Dubietis, R. Piskarskas, A. Varanavičius, and A. Piskarskas, Opt. Lett. **29**, 1123 (2004).
[26] M. A. Porras, A. Parola, D. Faccio, A. Dubietis, and P. Di Trapani, Phys. Rev. Lett. **93**, 153902 (2004).
[27] J. Marburger, Prog. Quantum Electron. **4**, 35 (1975).
[28] P. Di Trapani, G. Valiulis, A. Piskarskas, O. Jedrkiewicz, J. Trull, C. Conti, and S. Trillo, Phys. Rev. Lett. **91**, 093904 (2003).
[29] G. Méchain, A. Couairon, M. Franco, B. Prade, and A. Mysyrowicz, Phys. Rev. Lett. **93**, 035003 (2004).
[30] T. Brabec and F. Krausz, Phys. Rev. Lett. **78**, 3282 (1997).
[31] A. V. Engen, S. Diddams, and T. Clement, Appl. Opt. **37**, 5679 (1998).
[32] M. Mlejnek, E. M. Wright, and J. V. Moloney, Opt. Lett. **23**, 382 (1998).